Single-cell RNA-sequencing redefines blood cell type classification in mosquitoes

Maiara S. Severo[1], Jonathan J.M. Landry[2], Randall L. Lindquist[3], Christian Goosmann[4], Volker Brinkmann[4], Paul Collier[2], Anja E. Hauser[3,5], Vladimir Benes[2], Sarah A. Teichmann[6], Elena A. Levashina[1,7*]

[1]Vector Biology Unit, Max-Planck-Institute for Infection Biology, Charitéplatz 1, 10117 Berlin, Germany

[2]Genomics Core Facility, European Molecular Biology Laboratories, Meyerhofstraße 1, 69117 Heidelberg, Germany

[3]Deutsches Rheumaforschungszentrum, Charitéplatz 1, 10117 Berlin, Germany

[4]Microscopy Core Facility, Max-Planck-Institute for Infection Biology, Charitéplatz 1, 10117 Berlin, Germany

[5]Immune Dynamics and Intravital Microscopy, Charité Universitätsmedizin, Charitéplatz 1, 10117 Berlin, Germany

[6]Wellcome Trust Sanger Institute and European Bioinformatics Institute, Wellcome Genome Campus, Hinxton, Cambridge, CB10 1SD, UK

[7]Lead contact

*Correspondence: levashina@mpiib-berlin.mpg.de

SUMMARY

Mosquito blood cells are ancestral immune cells that help control infection by vector-borne pathogens. Despite their importance, little is known about mosquito blood cell biology beyond the ambiguous morphological and functional criteria used for their classification. Here we combined the power of single-cell RNA-sequencing, imaging flow cytometry and single-molecule RNA hybridization to analyze blood cells of the malaria mosquito *Anopheles gambiae*. By demonstrating that blood cells express nearly half of the mosquito transcriptome, our dataset represents an unprecedented view into their transcriptional machinery. Analyses of differentially expressed genes identified transcriptional signatures of two distinct cell types that challenge the current morphology-based classification of these cells. We further demonstrated an active transfer of a cellular marker between blood cells that confounds their identity. We propose that cell-to-cell exchange is broadly relevant for cell type classification and may account for the remarkable cellular diversity observed in nature.

INTRODUCTION

The cell is the basic building block of all living organisms. All the major decisions coordinating systems at the organismal level, be it life or death, health or disease, start within a cell. In eukaryotes, multicellularity came with cell compartmentalization and specialization. Cells found in the blood, or hemolymph in invertebrates, have received numerous denominations, such as hemocytes, amebocytes, phagocytes, coelomocytes and immunocytes (Ottaviani and Franceschi, 1997). Regardless of their names, these cells play key roles in shaping the extracellular environment and helping fight infection all throughout the animal kingdom. In insects, blood cells are found circulating by the flow of hemolymph, or as sessile cells associated with internal organs (Ribeiro and Brehelin, 2006). These cells are considered the equivalent of leukocytes in mammals, and display extraordinary functional resemblances to neutrophils, monocytes and macrophages, e.g. phagocytic abilities, chemotaxis, production of antimicrobial peptides, free radicals and cytokine-like molecules (Bergin et al., 2005; Browne et al., 2013; Buchmann, 2014; Costa et al., 2005; Lavine and Strand, 2002). Contrary to the well-established classification of human leukocytes, blood cell type classification is controversial in insects, with similar terms being used for different cell morphologies even within the same insect order (Brayner et al., 2005; Castillo et al., 2006; Hernandez et al., 1999; Ribeiro and Brehelin, 2006).

55 Of note, most studies of insect blood cells have focused on the embryonic and larval stages of
56 the *Drosophila* model (Brandt et al., 2008; Vlisidou and Wood, 2015; Wood and Jacinto, 2007)
57 and these observations are not immediately applicable to other insects (Ribeiro and Brehelin,
58 2006; Zdobnov et al., 2002), particularly in the study of the adult life stages of insects implicated
59 in disease transmission to humans.

60 Mosquitoes are the deadliest animals on Earth, transmitting pathogens that cause a variety of
61 diseases and infect millions of people worldwide every year (WHO, 2014). While feeding on blood
62 to reproduce, adult female mosquitoes acquire blood-borne pathogens from an infected host.
63 Pathogen development and replication within the mosquito is an absolute requirement for further
64 transmission, so the disease cycle is, in part, determined by the mosquitoes' capacity to
65 counterattack these pathogens. Mosquito blood cells are of vital importance in this process as
66 they represent the cellular arm of mosquito immunity, and also participate in humoral responses
67 by secreting pathogen-killing factors, such as components of the melanization pathway (Hillyer et
68 al., 2003; Yassine et al., 2012) and of the complement-like system that help eliminate malaria
69 parasites (Blandin et al., 2004; Frolet et al., 2006). Earlier transcriptomics studies based on
70 microarrays have explored the molecular basis of mosquito hemocyte immunity upon infection
71 with bacteria and *Plasmodium* (Baton et al., 2009; Pinto et al., 2009). More recently, Smith et al
72 used mass spectrometry to analyze mosquito hemocytes isolated based on their uptake of
73 magnetic beads (Smith et al., 2016). To identify genes and proteins more predominantly
74 expressed in hemocytes or in 'phagocytes', these studies relied on enrichment analyses of blood
75 cells relative to whole body or total hemolymph samples, respectively. This restricted the
76 identification of genes co-expressed in blood cells and other tissues, and masked the contribution
77 of sessile hemocytes to overall systemic responses. Such approaches are standard in the study
78 of hemocyte biology, mainly due to the practical constraints associated with the scarcity of these
79 cells and the lack of cellular markers for successful hemocyte isolation and purification.

80 Importantly, the absence of cellular markers has also precluded the classification of mosquito
81 blood cells beyond morphology and function. To date, mosquito hemocytes are morphologically
82 divided based on label-free light microscopy into: (1) granulocytes, phagocytic cells that exhibit
83 granules in their cytoplasm and quickly spread onto glass; (2) oenocytoids, spherical and poorly
84 adhesive cells that produce phenoloxidases involved in melanization defenses; and (3)
85 prohemocytes, small cells of reportedly 2 μm (Rodrigues et al., 2010; Smith et al., 2015) or 4-6
86 μm in size that have been suggested to function as hemocyte progenitors (Castillo et al., 2006),
87 and/or represent small phagocytic cells arising from asymmetrical divisions (King and Hillyer,

88 2013). Although it has been demonstrated that mosquito hemocytes increase in numbers upon
89 blood feeding and infection, in the absence of known hematopoietic organs (Bryant and Michel,
90 2014; King and Hillyer, 2013), the pathways underlining their differentiation into these three
91 classes remain unknown. Whether the current classification represents true discrete cell types or
92 states, and if mosquito blood cell subpopulations exist, are also yet to be explored. In humans
93 and mice, single-cell transcriptomics have recently began to tackle similar questions. It is now
94 also increasingly evident that significant functional differences and considerable variability in gene
95 expression can be recognized in cells long considered to be of the same type (Gaublomme et al.,
96 2015; Grun et al., 2015; Shalek et al., 2014). The use of single-cell approaches to explore cellular
97 heterogeneity in non-model organisms holds the promise to uncover unforeseen complexity, and
98 identify cellular populations that would be forever 'masked' in bulk, enrichment-based
99 measurements. In addition, single-cell studies of invertebrates can contribute to comparative
100 analyses of cellular diversity across different systems.

101 Here we unravel the molecular fingerprint of a subset of mosquito blood cells at a single-cell level,
102 and show that naïve, unstimulated hemocytes express nearly half of the mosquito transcriptome.
103 Our dataset represents a valuable resource for further studies of transcriptional regulation in
104 mosquitoes, and paves the way for the identification of new molecules controlling infection by
105 vector-borne pathogens. By applying fluorescence-activated cell sorting (FACS), single-cell RNA-
106 sequencing (scRNA-seq) and high-throughput imaging flow cytometry to the analysis of mosquito
107 hemocytes, our unparalleled study identifies two distinct blood cell subpopulations. Remarkably,
108 the identified cell subsets do not directly correspond to the current morphological and functional
109 classification of mosquito blood cells, and indicate that the emerging observations of cellular
110 heterogeneity in humans and mice are also characteristic of ancestral blood cells. Our findings
111 further reveal active molecular exchange between mosquito blood cells and the presence of
112 extracellular vesicles (EVs) in the mosquito hemolymph. Shuffling of mRNA and proteins between
113 distinct cell types can influence cellular identity and, in turn, confound cell type identification and
114 classification. Altogether, we demonstrate the power of single-cell technologies in shedding light
115 on the contribution of cell-to-cell exchange to cellular diversity and provide a new perspective on
116 the discussion of the slippery concept of 'cell types'.

117

118

119 **RESULTS**

120 **Single-cell RNA-sequencing of blood cells from *PPO6::RFP* transgenic mosquitoes**

121 In the absence of hemocyte-specific antibodies and dyes, or of transgenic mosquitoes expressing
122 pan-hemocyte markers, we chose to explore a subset of blood cells identified in a transgenic
123 mosquito strain expressing a red fluorescence reporter (tdTomato, abbreviated herein as RFP)
124 under the control of the *prophenoloxidase 6* (*PPO6*) melanization-related gene (*PPO6::RFP*)
125 (Volohonsky et al., 2015). Melanization is a well-established immune response of invertebrates
126 that controls infection against bacteria and parasites (Abraham et al., 2005; Christensen et al.,
127 2005; Hillyer and Strand, 2014; Michel et al., 2005). Several reports suggest that melanization is
128 mediated by a specific cell population called oenocytoids, which represents approximately 10%
129 of the blood cells (Castillo et al., 2006; Hillyer and Strand, 2014), but these cells have not been
130 directly explored. Our focus was on cells obtained in the absence of infection or blood feeding,
131 i.e. during homeostasis because it provides a baseline for analysis of cell-to-cell variation. Using
132 this transgenic strain, we first investigated whether RFP-positive hemocytes were present in the
133 mosquito circulation. For that, we perfused hemolymph onto microscope slides and identified cells
134 displaying RFP fluorescence within the size range predictive of hemocytes (Figure 1A). RFP
135 signal was also observed in hemocytes attached to the inner abdominal wall of dissected adult
136 female mosquitoes, where fat body cells are most prominent (Figure 1B, arrow). As expected, the
137 hemolymph perfusate was, however, heavily contaminated with a mixture of cells and
138 subcellular/tissue debris (Castillo et al., 2006). To purify live RFP-positive cells, we developed a
139 FACS approach based on RFP expression and Hoechst nuclear staining, and validated our
140 purification method by microscopic inspection of sorted cells (Figure 1C-D). Notably, the sorted
141 cell population corresponded to 0.1% of the total events measured (n=100,000) in the perfusate
142 of at least 10 mosquitoes (see Methods). This is in accordance with previous work indicating that
143 only a small subset of adult mosquito hemocytes produce PPOs (Hillyer and Strand, 2014).

144 Next, we FACS-sorted single blood cells and performed scRNA-seq to capture the transcriptome
145 of single PPO-producing blood cells (Figure 1E). Hemocytes were sorted into a 96-well plate and
146 after sample processing and quality assessment (see Methods), we obtained successful cDNA
147 amplification for 56 single-cells in addition to two pools of 30 cells each, from which 28 high quality
148 cDNA libraries were sequenced, representing 26 single hemocytes and the two pooled samples
149 (Figure S1A-D). As a single mosquito can contain as little as 500 blood cells in the circulation
150 (Bryant and Michel, 2014; Hillyer, 2010), we believe the small number of cells analyzed reflects a

151 combination of technical limitations inherent to our approach. First, blood cell isolation is not trivial
152 in mosquitoes, as it requires hemolymph perfusion under micromanipulation followed by cell
153 purification, posing great difficulty in obtaining high numbers of live cells. Second, mosquito blood
154 cells reportedly vary in size from as little as 2 to 20 μm (Brayner et al., 2005; Bryant and Michel,
155 2016; Castillo et al., 2006; Hernandez et al., 1999), and variability in cell size can significantly
156 affect RNA recovery, as small cells contain small amounts of RNA. The adaptation of the scRNA-
157 seq protocol to the study of an invertebrate system, e.g. the choice of lysis buffer and chemistry,
158 may also have influenced our results, especially since different biological cell types show distinct
159 technical quality features in scRNA-seq experiments (Ilicic et al., 2016). A small number of cells
160 has, nevertheless, been used in other scRNA-seq studies (Shalek et al., 2013; Xue et al., 2013)
161 and does not preclude identification of cellular types when an adequate sequencing depth is used.
162 We, therefore, prioritized the deep sequencing of individually curated, very high-quality samples
163 representing a small subset of cells obtained *ex vivo*.

164 Indeed, our sequencing generated on average 4.5 million reads per sample, well-above the
165 minimum of one million reads previously suggested as a requirement for adequate single-cell
166 studies (Wu et al., 2014). Over 70% of the reads were successfully mapped, with exonic reads
167 comprising of more than 40% (Figure S1E-F and Table S1). All samples achieved saturation at
168 around 2 million reads, comparable to previously observed for mammalian cells (Wu et al., 2014).
169 For further analyses, we discarded one cell as it showed gene expression suggestive of a doublet
170 (Figure S1F). Doublets have been reported in the circulation of adult female mosquitoes (King
171 and Hillyer, 2013) and may fall within a size range comparable to larger hemocytes. Around 3,800
172 genes were detected in each pool, whereas single-cells expressed between 450 and 1,400 genes.
173 Similar expression profiles were obtained for pools and single-cells (Figure 1F) with comparable
174 numbers of detected genes only in single-cells or in the pools (1,100 and 1,200 genes,
175 respectively) (Figure 1G). The marker genes used for FACS-sorting (*PPO6* and *tdTomato*) were
176 identified in both single-cells and pools (Table S2), confirming the efficiency of our method.
177 Altogether, our results show that the transcriptome of mosquito hemocytes comprises of over
178 6,000 genes, of which more than half (3,400) had not been identified in earlier studies (Figure
179 S1G) (Baton et al., 2009; Pinto et al., 2009). In addition, our approach revealed sequences for
180 over 80% (n=914) of the proteins reported by an earlier proteomics approach based on magnetic
181 beads isolation of *A. gambiae* phagocytes (Smith et al., 2016) (Figure S1H), corroborating our
182 findings and demonstrating the higher sensitivity of RNA sequencing as compared to proteomics.

183 Mosquito hemocyte biology has been mostly studied in the context of immunity. We, thus,
184 inspected our dataset for previously identified immune genes. Several members of immune
185 pathways were expressed at low levels in some naïve hemocytes, such as the transcription
186 factors *REL1* (AGAP009515) and *REL2* (AGAP006747), *Cactus* (AGAP007938),
187 *IκBβ* (AGAP009166) and *IκBγ* (AGAP005933), and the receptors *PGRP-LC* (AGAP005203) and
188 *PGRP-S1* (AGAP000536) (Table S2). Components of the complement cascade, e.g. *TEP1*
189 (AGAP010815), *APL1C* (AGAP007033), *LRIM1* (AGAP006348) and *HPX2* (AGAP009033), were
190 also detected in some cells, along with the LPS-induced TNFα transcription factor (LITAF)-like 3
191 (AGAP009053) described to control *Plasmodium* survival in the gut (Smith et al., 2015). The
192 phagocytic and antibacterial activities of these cells can be illustrated by the expression of *Eater*
193 (AGAP012386), *Ninjurin* (AGAP006745) and *Nimrod* (AGAP009762), alongside that of several
194 fibrinogen-related proteins (FREPs/FBNs), such as *FBN8* (AGAP011223), *FBN9* (AGAP011197),
195 *FBN10* (AGAP011230) and *FBN30* (AGAP006914) (Dong and Dimopoulos, 2009; Estevez-Lao
196 and Hillyer, 2014; Lombardo et al., 2013). Although no ortholog for a major *Drosophila* hemocyte
197 marker, hemolectin, has been described in the *A. gambiae* genome, mosquito hemocytes
198 expressed both *Pannier* (AGAP002235) and *Serpent* (AGAP002238) GATA factors, as well as
199 *misshapen* (AGAP006340), which are associated with blood cell differentiation, maturation and
200 activation in fruit fly larvae (Braun et al., 1997; Fossett et al., 2003; Minakhina et al., 2011). Genes
201 involved in cell adhesion and polarity, such as *integrin β-1* (AGAP010233), *laminin*
202 (AGAP010548), *Notch1* (AGAP001015) and *Armadillo* (AGAP001043), and components of
203 extracellular matrix like *collagen type IV* (AGAP009200) were also identified. The processed
204 expression data for single gene visualization is accessible at http://data.teichlab.org. Our
205 transcriptional data suggests that in addition to immunity, naïve blood cells are performing tissue
206 maintenance and morphogenesis tasks.

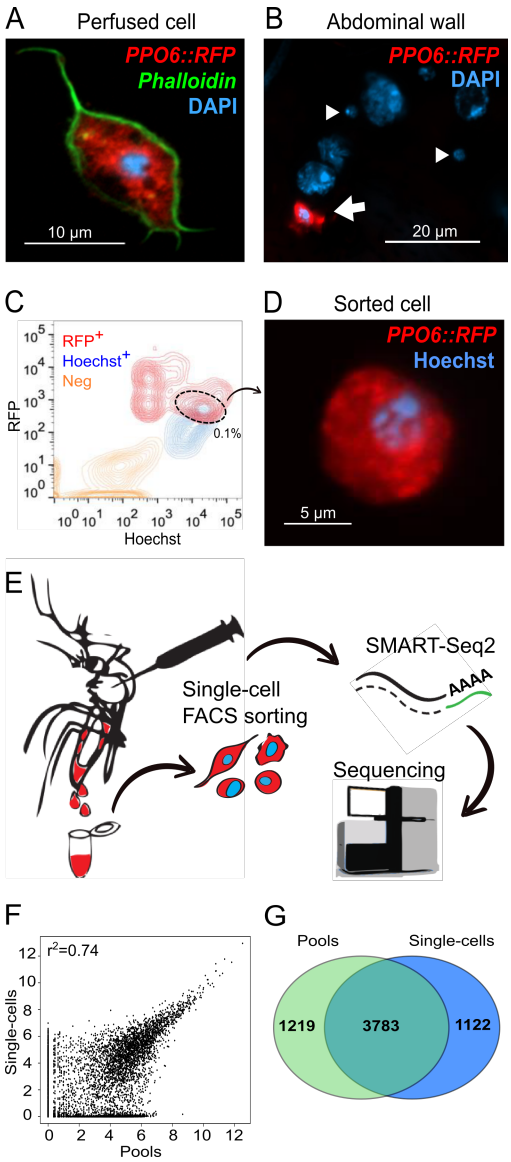

Figure 1: Single-cell RNA-sequencing of transgenic mosquitoes expressing a RFP reporter. A *PPO6::RFP* transgenic mosquito strain was used for isolation of blood cells. (A) A RFP-expressing hemocyte (red) obtained by perfusion of a female adult mosquito. (B) Only a proportion of adult mosquito blood cells display RFP expression (red, arrow), whereas other cells of sizes suggestive of hemocytes do not (arrowhead). (C) FACS sorting of RFP^+ (R^+) $Hoechst^+$ (H^+) blood cells from hemolymph of perfused *PPO6::RFP* mosquito females. (D) Representative image of a sorted cell. (E) The pipeline developed for the study of mosquito blood cells based on single-cell RNA-sequencing. Cells were sorted into a 96-well plate, processed according to the SMART-Seq2 protocol and sequenced in a HiSeq Illumina platform. (F) Scatter plot for the average normalized read counts from pools and single-cells. r^2 indicates Pearson correlation. (G)

218 Venn diagram of genes detected in single-cells and pools (normalized count ≥ 1). Scale bars: (A)
219 10 μm, (B) 20 μm, (D) 5 μm. DNA is stained with DAPI (A-B) and Hoechst (D).

220

221 **Identification of blood cell subpopulations**

222 To account for the technical noise arising from the small amounts of RNA, we included in our
223 samples External RNA Controls Consortium spike-ins (ERCC) prior to cDNA amplification (Baker
224 et al., 2005). We analyzed percentage of spike-ins and mitochondrial counts as a proxy for
225 sequencing efficiency, RNA degradation or incomplete lysis and potential cell death. As
226 anticipated, variation was observed (Figure S1I-J), but caution was taken in applying these criteria
227 and attributing them biological meaning because variability could have arisen from true cell type-
228 related processes. Differences in total number of expressed genes could also have stemmed from
229 different morphologies and cell types. Therefore, we decided not to further discard any cells, and
230 manually curated their individual mappings to confirm that the samples corresponded to
231 potentially true representations of mosquito blood cells. To estimate technical noise, we applied
232 the variability threshold based on the square of the coefficient of variation (CV^2) of the spike-ins
233 (Brennecke et al., 2013), and identified 148 genes whose expression exceeded the variability
234 threshold modeled by the spike-ins (Figure 2A). These highly variable genes included a
235 scavenger receptor, fibrinogen-related and leucine-rich repeat-containing proteins, as well as
236 genes involved in vesicle transport, metabolism and transcription (Table S3). No genes directly
237 associated with cell cycle had high variability, although several *cyclin* genes were detected in
238 specific cells (Table S2), corroborating previous reports of the potential of mosquito hemocytes
239 to undergo cellular division (Bryant and Michel, 2014, 2016; King and Hillyer, 2013).

240 Considering the variable genes, we carried out hierarchical clustering based on pairwise Pearson
241 correlation, which suggested the presence of at least two groups of mosquito blood cells in our
242 samples (Figure 2B). Principal component analysis (PCA) also yielded two cell populations,
243 supporting our clustering results (Figure 2C). Interestingly, the expression levels of *PPO6* showed
244 high variability, and the overlay of *PPO6* expression onto the PCA plot suggested that the two
245 clusters were largely characterized by low and high expression of *PPO6*. Differences in the *PPO6*
246 expression levels have been previously described by immunofluorescence microscopy (Bryant
247 and Michel, 2016) but have not been associated with cell types. Moreover, from the ten *PPO*
248 genes encoded in the *A. gambiae* genome, eight were observed in our sequencing and six of

249 them, as well as the *RFP* reporter, had variable expression between individual cells and the
250 groups (Figure 2D and Table S3). Hence, we designated these two groups as PPO6^{high} and
251 PPO6^{low}.

252

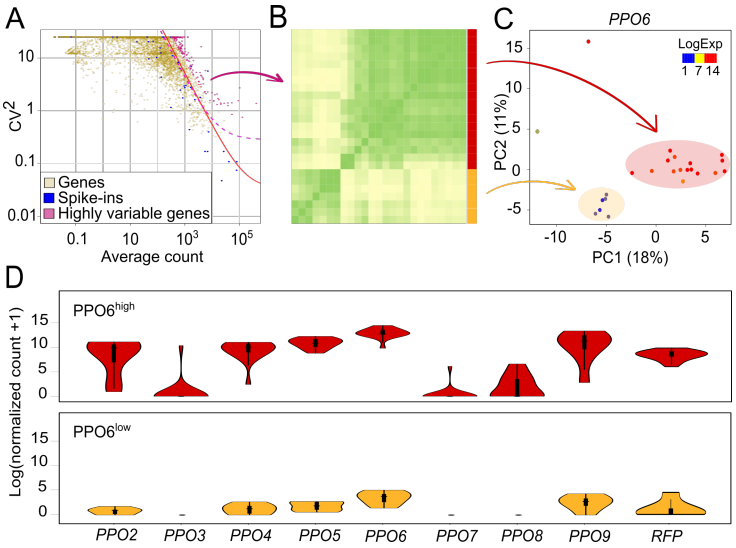

253

254 **Figure 2: Identification of mosquito blood cell subpopulations.** (A) The expression variability
255 of individual genes measured by the squared coefficient of variation (CV^2) is plotted against the
256 mean expression level (normalized counts). Magenta points indicate mosquito genes showing
257 higher than expected expression variability compared with ERCC spike-ins (blue) (adjusted *p*
258 value <0.1). The red line is the fitted line of the spike-ins and the dashed line (pink) marks the
259 margin for genes with 50% biological CV. (B) Pearson correlation heatmap of single hemocytes
260 based on the expression of the highly variable genes identified in (A). Correlation suggests the
261 presence of two groups of cells (red and yellow). (C) PCA plot based on the expression of highly
262 variable genes. The first two principal components are shown, and each point represents one
263 single hemocyte. Two clusters were identified and correspond to the subgroups in (B). *PPO6*
264 expression, as log10 (normalized counts +1), is overlaid onto the PCA plot. (D) Violin plots of
265 *PPOs* and *RFP* expression in the identified groups.

266

267

268

269 **PPO6^{high} and PPO6^{low} cells represent transcriptionally distinct subpopulations**

270 Among the highly variable genes, we detected several *FBN* sequences, such as *FBN8*, *10* and
271 *30*. PPO6^{high} cells showed high expression levels of *FBN10* (Figure 3A, left panel), whereas
272 PPO6^{low} cells exhibited weak or lack expression of *FBN8*, *10* and *30* (Figure 3A, Table S3).
273 Although below the ERCC-defined variability threshold, likely due to the small number of cells
274 analyzed, expression of the antimicrobial peptide gene *lysozyme type I* (*LysI*) (AGAP011119) was
275 more characteristic of PPO6^{low} cells (Figure 3A, middle panel). In the search for a pan-hemocyte
276 marker, we also identified expression of phagocytic receptor *Nimrod* in both groups of cells
277 (Figure 3A, right panel). To validate the *in silico* data, we performed single-molecule RNA
278 fluorescence *in situ* hybridization (RNA-FISH), and observed co-expression of *tdTomato* and
279 *PPO6* in all *PPO6::RFP* hemocytes, with no detection of *tdTomato* in blood cells isolated from
280 wild-type mosquitoes (Figure S2A-B, and data not shown). In terms of *PPO6* levels, RNA-FISH
281 accurately distinguished PPO6^{high} and PPO6^{low} hemocytes, confirming our bioinformatics results.
282 Consistently, PPO6^{high} cells showed high levels of *FBN10*, which were very low or absent in
283 PPO6^{low} cells. High levels of *LysI* were found in PPO6^{low} cells, reinforcing the presence of
284 PPO6^{low}/FBN10^{low}/LysI^{high} cells; and *Nimrod* was near ubiquitously expressed in all perfused
285 hemocytes (Figure 3B). We took advantage of the high conservation levels of *PPO6*, *LysI* and
286 *Nimrod* in the closely related mosquito species, *Anopheles stephensi*, the Asian malaria vector,
287 to explore whether the newly discovered blood cell subgroups were present in other anopheline
288 mosquitoes. Indeed, PPO6^{high} and PPO6^{low}/LysI^{high} cells were seen, along with a low degree of
289 expression of *Nimrod*. No *FBN10* was measured (Figure S2C), probably due to the specificity of
290 the probe to *A. gambiae* and the large diversity of this gene family.

291 To obtain the transcriptional signatures of PPO6^{high} and PPO6^{low} cells, we compared the overall
292 gene expression between these two groups. Based on differentially expressed genes, gene
293 ontology (GO) analyses uncovered that melanization characterized PPO6^{high} cells, whereas
294 metabolism and RNA processing defined the PPO6^{low} subset (Table S4). Although not significant,
295 PPO6^{low} cells appeared to express more genes in total, but mitochondrial counts did not differ
296 between the groups (Figure S2D). These findings suggest that PPO6^{high} cells are specialized for
297 melanization responses, expressing genes involved in these processes at very high levels,
298 whereas PPO6^{low} cells execute a broader range of biological tasks, including melanization. An
299 alternative explanation would be that these groups represent different cell lineages, or perform
300 melanization for diverse processes, e.g. metamorphosis and cuticle sclerotization, as established
301 in other insects (Dudzic et al., 2015; Tsao et al., 2015; Tsao et al., 2009). Transcriptional

302 differences between the two groups could also reflect localization patterns of the cells inside the
303 mosquito body, as blood cells can be found in the circulation or attached to internal organs (King
304 and Hillyer, 2013) and sessile cells could have been displaced during hemolymph perfusion. To
305 assess whether observed differences were related to tissue residency, we performed RNA-FISH
306 in tissues. The analyses of sessile cells revealed both cell populations in close contact with fat
307 body cells within the abdominal wall with no conspicuous cell clusters. The majority of the sessile
308 cells were positive for *Nimrod*, independent of their *PPO* expression (Figure 3C), indicating that
309 *Nimrod* is a potential marker for both circulating and tissue-resident blood cells. Altogether, these
310 results demonstrate that both circulatory and tissue-resident hemocytes display transcriptional
311 heterogeneity, and that $PPO6^{high}$ and $PPO6^{low}$ cell populations are present in two mosquito
312 species.

313

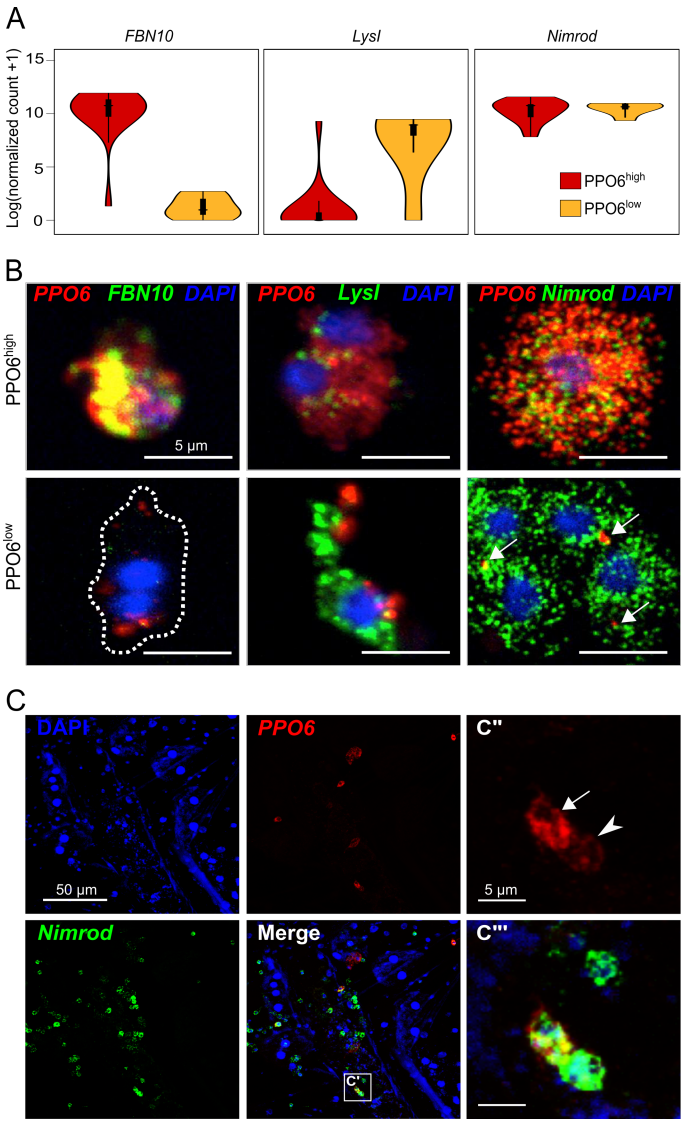

314

315 **Figure 3: Characterization of PPO6^{high} and PPO6^{low} cell subpopulations.** (A) Violin plots of
316 the expression of putative population and pan-hemocyte markers. (B) RNA-FISH validation of
317 identified PPO6^{high} and PPO6^{low} cell subpopulations in perfused cells based on markers shown in
318 (A). Cells were classified as PPO6^{high} (upper panel) or PPO6^{low} (lower panel) according to the
319 expression of *PPO6* (red). Arrows indicate lower *PPO6* signal. (C-C''') PPO6^{high} and PPO6^{low} cell
320 subpopulations can also be seen as tissue-resident blood cells attached to the inner abdominal
321 wall of female mosquitoes. Arrow and arrowhead indicate PPO6^{high} and PPO6^{low} cell
322 subpopulations, respectively. Scale bars: (B) 5 µm, (C) 50 µm, (C''-C''') 5 µm. DNA is stained with
323 DAPI.

324

325 **PPO6^{high} and PPO6^{low} cells share functional and morphological features**

326 Mosquito blood cells are functionally and morphologically separated into three classes -
327 granulocytes, oenocytoids and prohemocytes - based on microscopic studies of surface-attached
328 cells. Our GO analyses suggested the presence of a PPO-specialized cell population and a
329 second cell subset of a less specific nature. Based on that, we reasoned that PPO6^{high} and
330 PPO6^{low} cell groups could be representatives of oenocytoids and granulocytes, respectively. As
331 phagocytosis is a hallmark of granulocytes, we first explored functional differences between these
332 cells using magnetic bead uptake as means for "phagocyte" isolation, as suggested before (Smith
333 et al., 2016). To this end, we injected mosquitoes with magnetic beads and either allowed them
334 to rest at 28°C prior to hemolymph perfusion or incubated the mosquitoes at 4°C to inhibit
335 phagocytosis. To our surprise, both PPO6^{high} and PPO6^{low} cells were identified among
336 magnetically isolated cells and under both conditions, suggesting that instead of phagocytosis,
337 both cell types endocytosed the beads, as no differences in bead uptake were observed when
338 this assay was performed under cold conditions (Figure 4A, arrows). To confirm these findings,
339 we compared the gene profiles of PPO-producing cells to the proteomics results obtained by
340 Smith et al using magnetic bead isolation at 28°C only (Smith et al., 2016). Our analyses revealed
341 that similarities were the strongest when profiles were compared across all samples - PPO6^{high},
342 PPO6^{low}, phagocytes and all cells, i.e. unselected cells obtained in the absence of magnetic
343 isolation. PPO6^{high} and PPO6^{low} shared expression of more genes with phagocytes when
344 considered together rather than alone, indicating that neither PPO6^{high} and PPO6^{low} cell types
345 shared striking similarities with phagocytes at the gene/protein level (Figure 4B). In agreement,
346 nearly all PPOs were present in all samples (Figure 4B'). Overall, these findings did not detect
347 functional differences between PPO6^{high} and PPO6^{low} cells. We conclude that endocytic
348 capabilities likely characterize both granulocytes, considered the "true" phagocytic cell type, and
349 oenocytoids, known as the major source of PPOs.

350 Next, we sought to investigate whether the identified cell populations could be distinguished
351 based on their morphology using imaging flow cytometry and RFP fluorescence as a proxy for
352 *PPO6* expression. We measured a series of morphological features of 319 single RFP-positive
353 cells, which could be divided into RFP^{high} (PPO6^{high}, n=58) and RFP^{low} (PPO6^{low}, n=261) based
354 on their fluorescence intensity (Figures 4C-D and Figure S3). Overall, RFP-positive cells had a
355 mean area of approximately 67 μm^2, ranging from 18 μm^2 to nearly 140 μm^2. These
356 measurements are in accordance with cell sizes reported elsewhere (Bryant and Michel, 2014,
357 2016; Castillo et al., 2006). Similar to recent studies based on flow cytometry of fixed cells (Bryant

358 and Michel, 2014, 2016), we did not detect the cells of 2 μm in size described by other research
359 groups based on label-free light microscopy alone (Rodrigues et al., 2010; Smith et al., 2015).
360 When comparing the cell groups in terms of bright-field measurements of their cytoplasm (see
361 Methods), PPO6^{low} cells showed smaller cytoplasmic area, width, and minor axis than PPO6^{high}
362 cells (Figure 4E and Figure S3). No differences between the groups were detected in granularity
363 or cell shape (Figure S8 and Table S5). To our surprise, PPO6^{high} and PPO6^{low} cells were equally
364 circular. At times, cells from both groups also displayed an elongated shape, typical of the
365 cytoplasmic extensions seen in fusiform or spindle-shaped cells. This fusiform shape is
366 characteristic of plasmatocytes, described in other insects (Ribeiro and Brehelin, 2006). These
367 results failed to morphologically assign RFP-positive cells to any of the morphologically-defined
368 groups: granulocytes, plasmatocytes, or oenocytoids. In fact, the highest discriminating factors
369 (Fisher's linear discriminant, see Methods) separating PPO6^{high} and PPO6^{low} subpopulations
370 relied on RFP intensity alone, with bright-field parameters scoring poorly and failing to establish
371 a morphological distinction between the cells (Table S6). Importantly, our imaging flow cytometry
372 approach relied on morphological analyses of cells in suspension, which is unbiased and likely
373 more relevant for the identification of the cellular types found in the hemolymph circulation. This
374 might explain differences obtained relative to previous studies that focused on cells attached to
375 glass slides, which might be rather reflective of cell 'states' driven by activation of the cellular
376 attachment and adhesion machineries upon exposure to electrostatically charged glass.

377 In addition to RFP intensity, the cell groups differed in their RFP area. PPO6^{high} cells displayed
378 an overall cytoplasmic distribution of the RFP signal, whereas a more localized and globular signal
379 was detected in the cytoplasm of PPO6^{low} cells, where RFP lobes were also more numerous,
380 reinforcing the localized nature of the RFP signal (Figure 4D-E). Microscopic examination also
381 revealed that nearly half of the cells from both groups displayed internal structures and or
382 "budding" extensions of the cytoplasm suggestive of vesicles (Figure 4F-G, arrowhead and arrow,
383 respectively). To confirm that, we performed correlative scanning electron microscopy (SEM) and
384 demonstrated the presence of membrane protrusions or "blebs" in RFP-positive cells (Figure
385 S4A). Altogether, these results established that morphological plasticity of the mosquito blood
386 cells is independent from their transcriptional profile, and that mosquito blood cells have
387 membrane vesicles and protrusions.

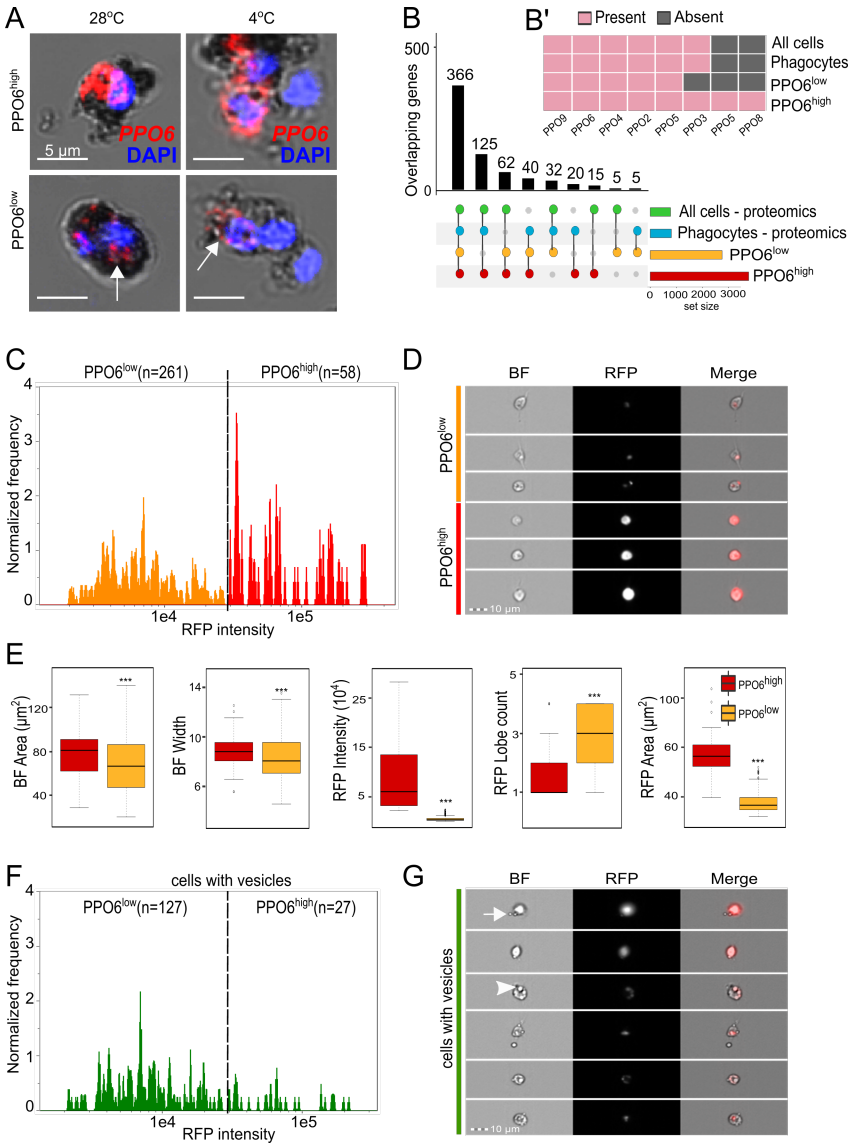

Figure 4: PPO6^{high} and PPO6^{low} cell subpopulations share functional and morphological features. (A) Magnetic bead isolation assays followed by RNA-FISH for identification of cell subpopulations. Arrows indicate lower *PPO6* signal. (B) Intersection analyses between PPO6^{high} and PPO6^{low} cell subpopulations and proteomics results obtained by Smith et al for phagocytes and all cells (unselected). Presence or absence of PPO genes/proteins in each of the samples in shown in (B'). (C) Hemocytes were perfused from *PPO6::RFP* mosquitoes and analyzed using imaging flow cytometry. RFP-positive cells were identified by their RFP Median Pixel and further separated into PPO6^{high} and PPO6^{low} based on their level of RFP fluorescence. The number of cells analyzed per group is shown between parentheses and the dotted line indicates the RFP threshold level used for separation of the two populations. (D) Image gallery containing

399 representative images of PPO6^{high} and PPO6^{low} populations. Variation in cell shape and RFP
400 intensity can be observed in the bright field (BF), RFP and merged images. (E) For every event
401 measured within the flow, a corresponding image and fluorescence levels were acquired and
402 analyzed to generate multiple morphological features. Boxplots show the distribution of five
403 morphological measurements according to the groups. Asterisks represent $p < 0.01$ based on
404 Mann-Whitney-Wilcoxon test. (F) RFP-positive cells were interrogated for the presence of
405 membrane protrusions or internal structures suggestive of vesicles. Similar to (C), cells were
406 grouped into PPO6^{high} and PPO6^{low} and a RFP intensity histogram of cells displaying vesicles
407 (green population) was generated to illustrate that vesicles are observed in cells from both groups.
408 Representative images of cells in this population subset are shown in (G). Arrow and arrowhead
409 indicate representative membrane protrusions and internal vesicles, respectively. See also Figure
410 S4 and Tables S4-5. Boxplots indicate the median, first and third quartile, and min and max
411 values.

412

413 **Mosquito blood cells exchange molecular information**

414 Mosquito hemocytes have been described to produce and secrete EVs (Castillo et al., 2017;
415 Hillyer and Christensen, 2002) and, in agreement, our initial observation suggested that PPO-
416 producing cells display vesicles. We were, therefore, puzzled by the possibility that the RFP signal
417 analyzed in our cell sorting approach could have partially originated from RFP-positive vesicles.
418 Earlier reports used DiD, a lipophilic cyanine dye, to label both mosquito hemocytes and
419 hemocyte-derived vesicles (Castillo et al., 2017; King and Hillyer, 2012). To test whether the
420 localized RFP signal seen in our imaging flow cytometry was associated with vesicles, we first
421 stained PPO-producing cells with DiD and observed that RFP-positive cells indeed contained
422 DiD-positive membrane-bound and internal vesicles that were both RFP-positive and negative
423 (Figure S4B-C). Recently, it has also become clear that EVs are present in extracellular fluids like
424 milk, saliva and plasma, so we reasoned that EVs might be also found in the hemolymph and in
425 association with RFP-negative cells. To identify EVs in the mosquito circulation, we performed
426 imaging flow cytometry analyses using DiD and a recently published approach (Headland et al.,
427 2014). Both DiD-positive cells and EVs could be identified in hemolymph perfusate (Figure 5A-
428 B). EVs were detected based on their small size, weak dark-field and positive DiD fluorescence,
429 with a few EVs also displaying weak RFP signal (Figure 5B, arrowhead). The degree of DiD
430 intensity differed between cells and did not depend on RFP fluorescence. Differential

431 centrifugation followed by electron microscopy confirmed the presence of EVs in hemolymph
432 perfusate of naïve female mosquitoes (Figure 5C). Moreover, SEM of perfused cells also revealed
433 that vesicles of different sizes and shapes, suggestive of the different vesicle types described in
434 the literature - exosomes, microvesicles and apoptotic vesicles (van der Pol et al., 2012), could
435 be indeed observed in association with naïve mosquito blood cells (Figure S4D). These findings
436 suggested that extracellular vesicle production is a general phenomenon that is not limited to
437 PPO-associated cells.

438 A growing body of evidence has demonstrated that RNA can be transferred between mammalian
439 cells. As RNA can be found in EVs, and our data showed that EVs are present in the mosquito
440 hemolymph, we decided to take a step further and explore the possibility that a crosstalk between
441 PPO-positive and negative cells could be responsible for the identification of $PPO6^{high}$ and
442 $PPO6^{low}$ cells. Strengthening this idea were the observations that (1) our scRNA-seq results
443 uncovered cells with minute levels of *PPO6* and *RFP*, and (2) expression of *PPO6* by RNA-FISH
444 was detected inside "budding" extensions associated with PPO6-positive cells (Figure 5D). As a
445 proof of concept, a transwell assay using blood cells from *PPO6::RFP* transgenic and wild-type
446 mosquitoes was developed to test the possibility that RFP mRNA can be transferred between
447 naïve transgenic and wild-type blood cells (Figure 5E). Remarkably, *RFP* transcripts were
448 observed by RNA-FISH inside wild-type blood cells after exposure to hemolymph perfusate from
449 transgenic mosquitoes (Figure 5F, arrowhead). This result indicated that *RFP* mRNAs can be
450 shuttled between blood cells and might account for the $PPO6^{low}$ cell population uncovered by our
451 scRNA-seq and imaging approaches. Taken together, our findings demonstrated that molecular
452 exchange between cells, likely via EVs, can affect their transcriptional profile. As EVs have been
453 shown to carry lipids, proteins and RNA, and can be secreted by virtually all cells, our results
454 revealed an unappreciated role of intercellular molecular exchange in defining cellular identity.

455

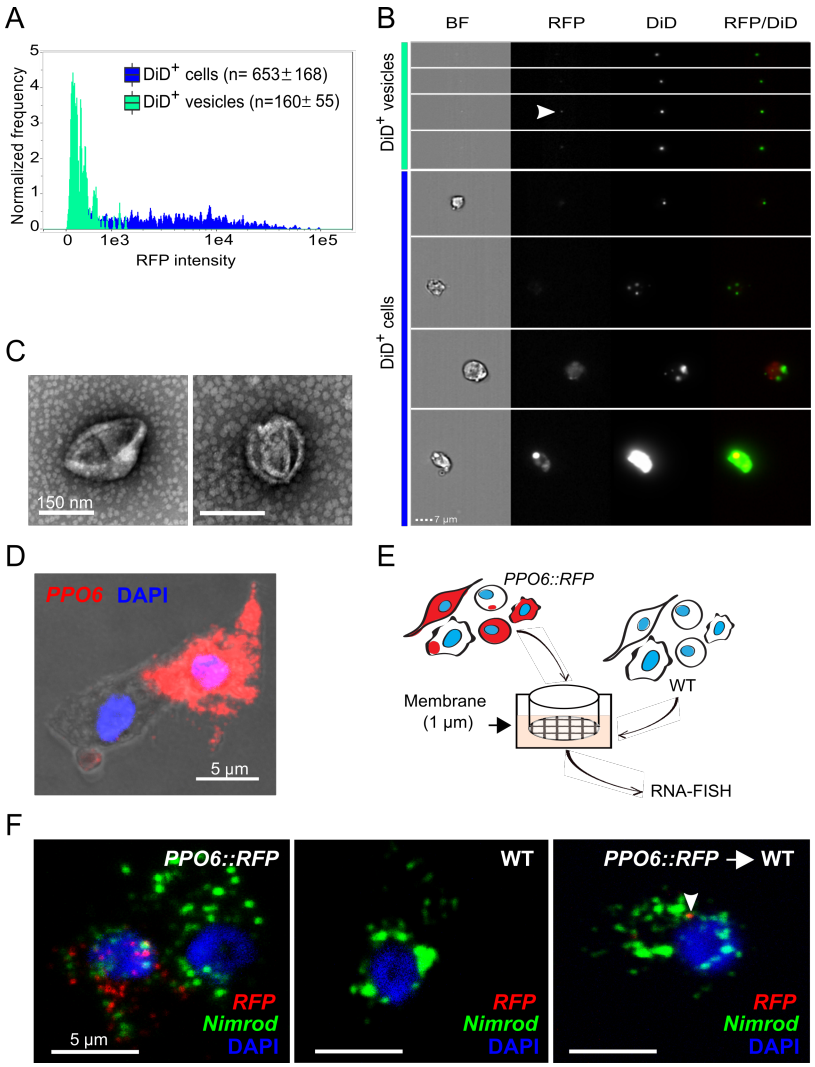

Figure 5: Vesicle identification and molecular exchange in mosquito blood cells. Hemocytes were perfused from *PPO6::RFP* mosquitoes, stained with the lipophilic DiD dye and analyzed using imaging flow cytometry. DiD-positive cells and EVs were first identified according to their DiD and darkfield intensity. EVs were further separated from cells based on their small bright field area. Cells were identified considering their area and aspect ratio. A RFP fluorescence histogram for both DiD-positive cells and EVs in shown in (A). (B) Representative images of DiD-positive cells and EVs. Arrowhead indicates a representative of a RFP-positive vesicle. (C) Negative staining electron microscopy of vesicles obtained by differential centrifugation (10,000xg) of hemolymph perfusate (representative images of 2 independent experiments are shown). (D) *PPO6* mRNA detection by RNA-FISH within budding extensions of blood cells. (E) Schematics of a transwell assay developed to test the transfer of *RFP* between blood cells from *PPO6::RFP* transgenic mosquitoes and wild-type mosquitoes that do not express any reporter

genes. Hemolymph perfusate from wild-type mosquitoes was pipetted onto a coverslip placed under a 1 µm membrane. Perfusate collected from *PPO6::RFP* mosquitoes was placed on top of the membrane. (F) RNA-FISH was performed on coverslips obtained from the transwell assay described in (E) using probes to detect *RFP and Nimrod* expression in wild-type acceptor cells (right panel, arrowhead). Representative images of 2 independent experiments are shown. See also Figure S4.

DISCUSSION

Understanding how transcriptional networks influence cell identity is a central problem in modern molecular biology. Our study describes mosquito blood cells as a source of key components of immunity, development and tissue homeostasis, and places these cells as a central hub coordinating mosquito biology at different levels. Using a combination of single-cell genomics and imaging, we revealed that hemocytes display an unexpected degree of complexity where two transcriptionally defined cellular 'populations' suggestive of distinct cell types share morphological and functional features. We also demonstrate that mosquito blood cells exchange mRNA, leading to the detection, by RNA-FISH, of an "exogenous" gene in acceptor cells. Altogether, our results open a new perspective on cellular crosstalk and cell type classification, in addition to illustrating the power of single-cell-based approaches in discovering unappreciated events at the core of biological processes.

Using single-cell RNA sequencing, we describe the baseline expression of a mosquito blood cell in exceptional detail. An average mosquito blood cell under resting conditions expresses approximately 1,000 genes, or 7% of the mosquito transcriptome. In total, about half of the genes currently annotated in the mosquito genome were detected by RNA sequencing naïve, unstimulated mosquito hemocytes. This represents a substantial gene expression resource for further studies of tissue-specific alternative splicing, RNA editing, gene and transcript models. It will also enable the establishment of transcriptional and regulatory networks that allow for more precise gene enrichment and functional studies. In mosquitoes, where tissue-specific gene knockdown is not available and transgenesis remains limited, functional analyses have greatly relied on the use of dsRNA injections into the open body cavity. This technical limitation restricts the interpretation of tissue-specificity of signaling pathways and their regulation. We believe our dataset will illustrate the importance of tissue specificity studies and pave the road towards the

500 detailed mapping of gene expression in cells and tissues of different systems, with the ultimate
501 goal of creating a comprehensive reference atlas of cellular diversity.

502 By successfully applying single-cell RNA sequencing to the study of blood cells involved in
503 immunity in a major malaria vector, we demonstrated proof of the existence of at least two
504 transcriptionally distinct cell subpopulations that do not represent currently defined cell types. Our
505 results show that the majority of *Anopheles* blood cells likely belong to the PPO6^{low} type. Their
506 rich transcriptional program appears to be reminiscent of granulocytes. The second
507 subpopulation, with a transcriptional profile specialized in melanization, is suggestive of
508 oenocytoids. Nonetheless, these two transcriptionally defined cell types could not be
509 distinguished by the customary functional or morphological tests. Therefore, we suggest to call
510 them plasmatocytes and melanocytes. Interestingly, only one cell type, plasmatocytes, is
511 described in the adult *Drosophila* flies. Our transcriptional definition of mosquito blood cells
512 redefines the obscure cellular classification extensively used in studies of hemocytes, and is
513 particularly significant in the context of cellular proliferation and differentiation because mosquito
514 hemocyte lineages are still to be established. Given our results, it will be interesting to address
515 the spatial distribution of mosquito blood cells based on the markers identified here, especially as
516 no lymph glands or hematopoietic cell clusters have been described in mosquitoes. Tissue-
517 resident blood cells likely contribute to local responses and help regulate tissue-specific events.
518 This is exemplified by the recent discovery of macrophage subsets regulating electrical pulsing in
519 the mouse heart (Hulsmans et al., 2017), and of ovarian hemocytes that control collagen IV
520 secretion and germline stem cell niche maintenance in *Drosophila* (Van De Bor et al., 2015).
521 Evidence that cellular heterogeneity can be recognized by profiling single insect blood cells, often
522 called macrophage-like, emphasizes the notion that innate immune cells are far more
523 heterogeneous than previously thought. As macrophages, along with other immune cells, have
524 their evolutionary roots in similar cells in ancestral invertebrates (Buchmann, 2014; Dzik, 2014)
525 and new cell types arise as a result of evolutionary processes (Arendt et al., 2016), the study of
526 insect blood cells can help elucidate the origins of the immune system.

527 In humans and mice, distinct levels and patterns of fluorescence of cellular markers are widely
528 used in microscopy and flow cytometry as a means to cell type classification. Cellular crosstalk
529 may, however, affect such approaches. Acquisition of macrophage-derived “blebs” by
530 lymphocytes has been described, resulting in misrepresentation of lymphocytes as macrophages
531 in flow cytometry studies, and suggesting that these two cells may interact to control early
532 responses in the lymph node (Gray et al., 2012). More importantly, translation of transferred

533 mRNAs into functional proteins has been demonstrated before (Valadi et al., 2007) along with the
534 reprogramming of acceptor cells upon microvesicle-mediated exchange (Ratajczak et al., 2006).
535 It is, therefore, intriguing to consider that expression of specific cellular markers might be
536 influenced by EV uptake. In this scenario, signals sent via vesicles include protein-coding RNAs
537 that are normally absent in acceptor cells, which once translated, appear to be an endogenous
538 cellular marker characteristic of the donor cell population. This observation calls for a critical
539 reassessment of cellular markers by the scientific community. It is also imperative to investigate
540 whether certain protein-coding RNAs are preferentially exchanged compared to other RNAs found
541 in the cells. How *PPO6* and *RFP* transcripts, and potentially other *PPO* genes, contribute to the
542 function of acceptor cells is another exciting question. PPO proteins lack the signal peptides
543 required for their secretion, and it has been suggested that PPO6 is secreted by exocytosis as
544 cell rupture has not been observed (Bryant and Michel, 2016). It is plausible that PPO transcripts
545 are shed by professional melanocytes and processed by non-professional plasmatocytes that
546 locally activate melanization only under specific conditions, e.g. upon infection with specific
547 pathogens, or during wounding and tissue repair. Molecular signals exchanged between cells
548 can, thus, coordinate cellular plasticity and account for the diversity of functional subsets or
549 'hybrid' cells that express markers of different or multiple cell types.

550 The demonstration of mosquito blood-borne EVs indicates that different cells and tissues likely
551 communicate through vesicles secreted into the insect open circulatory system. Several recent
552 reports have suggested EV-mediated immune responses in dipteran insects. Exosome-like
553 vesicles containing virus-derived siRNAs have been identified in *Drosophila* and contribute to
554 systemic antiviral immunity (Tassetto et al., 2017). Apoptotic vesicles released by hemocytes in
555 the proximity of invading parasites have been implicated in anti-*Plasmodium* responses by
556 activating the complement pathway in *A. gambiae* mosquitoes (Castillo et al., 2017). Interestingly,
557 using a GFP reporter strain, Volohonsky et al recently reported that, the anti-malaria mosquito
558 complement-like factor TEP1 is predominately expressed in the fat body as a transcript, but at
559 the protein level it is found in hemocytes upon blood feeding and infection (Volohonsky et al.,
560 2017). The authors speculate this is due to the uptake by the blood cells of TEP1 attached to
561 bacterial cells. As only one plasmatocyte containing low levels of *TEP1* was identified in our
562 sequencing, we suggest that EV-mediated delivery of TEP1 (mRNA or protein) may better explain
563 these surprising findings. We propose that vesicles found in the mosquito hemolymph contain
564 proteins and transcripts that coordinate cell-to-cell and tissue communication not only in infection
565 but also under physiological conditions. Disturbance in homeostasis, be it by infection, metabolic

566 changes, tissue damage or stress, may further escalate secretion of vesicles containing an array
567 of different cargo that can be targeted to specific tissues and complement systemic responses.
568 This represents an outstanding parallel between insects and humans, where EVs found in human
569 body fluids can elicit changes in function and gene expression in target cells, and have a direct
570 role in processes like differentiation, neuronal signaling and cancer. We believe that, similar to
571 how environment, microbiota and genetic make-up influence phenotypic variation, cellular
572 exchange can also drive cellular identity and represents an inventive and unexplored way through
573 which nature coordinates who and what we are.

574

575 **ACKNOWLEDGMENTS**

576 The authors thank all members of the Vector Biology Unit for intellectual input and technical
577 support. The authors thank Dr. E. Marois (UPR9022 CNRS, U963 Inserm, France) for sharing the
578 transgenic *PPO6::RFP* line and acknowledge discussions funded by CNRS LIA "REL2 and
579 resistance to malaria". We thank Dr. K Müller (Humboldt University, Berlin) for providing
580 *Anopheles stephensi* mosquitoes. We are also grateful for the support provided by the Flow
581 Cytometry Core Facility (DRFZ/MPIIB, Berlin). Finally, the authors thank Dr. J. Henriksson
582 (Wellcome Trust Sanger Institute and EBI, UK) for the data sharing platform.

583

584 **AUTHOR CONTRIBUTIONS**

585 M.S.S. and E.A.L. conceived the study, designed the experiments, analyzed the data and wrote
586 the manuscript. M.S.S. performed all experiments with assistance from R.L.L. for the imaging flow
587 cytometry studies, C.G. and V.B. for the EM analyses, and P.C. for the scRNA-seq. M.S.S. and
588 J.J.M.L. performed bioinformatic analyses. A.E.H. provided infrastructure. V.B. and S.A.T.
589 provided expert input.

590

591 **DECLARATION OF INTERESTS**

592 The authors declare no competing interests.

593

594 **REFERENCES**

595 Abraham, E.G., Pinto, S.B., Ghosh, A., Vanlandingham, D.L., Budd, A., Higgs, S., Kafatos, F.C.,
596 Jacobs-Lorena, M., and Michel, K. (2005). An immune-responsive serpin, SRPN6, mediates
597 mosquito defense against malaria parasites. Proceedings of the National Academy of Sciences
598 of the United States of America *102*, 16327-16332.

599 Alexa, A., Rahnenfuhrer, J., and Lengauer, T. (2006). Improved scoring of functional groups from
600 gene expression data by decorrelating GO graph structure. Bioinformatics *22*, 1600-1607.

601 Arendt, D., Musser, J.M., Baker, C.V., Bergman, A., Cepko, C., Erwin, D.H., Pavlicev, M.,
602 Schlosser, G., Widder, S., Laubichler, M.D.*, et al.* (2016). The origin and evolution of cell types.
603 Nature reviews Genetics *17*, 744-757.

604 Baker, S.C., Bauer, S.R., Beyer, R.P., Brenton, J.D., Bromley, B., Burrill, J., Causton, H., Conley,
605 M.P., Elespuru, R., Fero, M.*, et al.* (2005). The External RNA Controls Consortium: a progress
606 report. Nat Methods *2*, 731-734.

607 Baton, L.A., Robertson, A., Warr, E., Strand, M.R., and Dimopoulos, G. (2009). Genome-wide
608 transcriptomic profiling of Anopheles gambiae hemocytes reveals pathogen-specific signatures
609 upon bacterial challenge and Plasmodium berghei infection. BMC genomics *10*, 257.

610 Bergin, D., Reeves, E.P., Renwick, J., Wientjes, F.B., and Kavanagh, K. (2005). Superoxide
611 production in Galleria mellonella hemocytes: identification of proteins homologous to the NADPH
612 oxidase complex of human neutrophils. Infection and immunity *73*, 4161-4170.

613 Blandin, S., Shiao, S.H., Moita, L.F., Janse, C.J., Waters, A.P., Kafatos, F.C., and Levashina,
614 E.A. (2004). Complement-like protein TEP1 is a determinant of vectorial capacity in the malaria
615 vector Anopheles gambiae. Cell *116*, 661-670.

616 Brandt, S.M., Jaramillo-Gutierrez, G., Kumar, S., Barillas-Mury, C., and Schneider, D.S. (2008).
617 Use of a Drosophila model to identify genes regulating Plasmodium growth in the mosquito.
618 Genetics *180*, 1671-1678.

619 Braun, A., Lemaitre, B., Lanot, R., Zachary, D., and Meister, M. (1997). Drosophila immunity:
620 analysis of larval hemocytes by P-element-mediated enhancer trap. Genetics *147*, 623-634.

621 Brayner, F.A., Araujo, H.R., Cavalcanti, M.G., Alves, L.C., and Peixoto, C.A. (2005).
622 Ultrastructural characterization of the hemocytes of Culex quinquefasciatus (DIPTERA:
623 Culicidae). Micron *36*, 359-367.

624 Brennecke, P., Anders, S., Kim, J.K., Kolodziejczyk, A.A., Zhang, X., Proserpio, V., Baying, B.,
625 Benes, V., Teichmann, S.A., Marioni, J.C*., et al.* (2013). Accounting for technical noise in single-
626 cell RNA-seq experiments. Nat Methods *10*, 1093-1095.

627 Browne, N., Heelan, M., and Kavanagh, K. (2013). An analysis of the structural and functional
628 similarities of insect hemocytes and mammalian phagocytes. Virulence *4*, 597-603.

629 Bryant, W.B., and Michel, K. (2014). Blood feeding induces hemocyte proliferation and activation
630 in the African malaria mosquito, Anopheles gambiae Giles. The Journal of experimental biology
631 *217*, 1238-1245.

632 Bryant, W.B., and Michel, K. (2016). Anopheles gambiae hemocytes exhibit transient states of
633 activation. Developmental and comparative immunology *55*, 119-129.

634 Buchmann, K. (2014). Evolution of Innate Immunity: Clues from Invertebrates via Fish to
635 Mammals. Frontiers in immunology *5*, 459.

636 Castillo, J.C., Ferreira, A.B.B., Trisnadi, N., and Barillas-Mury, C. (2017). Activation of mosquito
637 complement antiplasmodial response requires cellular immunity. Sci Immunol *2*.

638 Castillo, J.C., Robertson, A.E., and Strand, M.R. (2006). Characterization of hemocytes from the
639 mosquitoes Anopheles gambiae and Aedes aegypti. Insect biochemistry and molecular biology
640 *36*, 891-903.

641 Christensen, B.M., Li, J., Chen, C.C., and Nappi, A.J. (2005). Melanization immune responses in
642 mosquito vectors. Trends in parasitology *21*, 192-199.

643 Costa, S.C., Ribeiro, C., Girard, P.A., Zumbihl, R., and Brehelin, M. (2005). Modes of
644 phagocytosis of Gram-positive and Gram-negative bacteria by Spodoptera littoralis granular
645 haemocytes. J Insect Physiol *51*, 39-46.

646 Dobin, A., Davis, C.A., Schlesinger, F., Drenkow, J., Zaleski, C., Jha, S., Batut, P., Chaisson, M.,
647 and Gingeras, T.R. (2013). STAR: ultrafast universal RNA-seq aligner. Bioinformatics *29*, 15-21.

648 Dong, Y., and Dimopoulos, G. (2009). Anopheles fibrinogen-related proteins provide expanded
649 pattern recognition capacity against bacteria and malaria parasites. The Journal of biological
650 chemistry *284*, 9835-9844.

651 Dudzic, J.P., Kondo, S., Ueda, R., Bergman, C.M., and Lemaitre, B. (2015). Drosophila innate
652 immunity: regional and functional specialization of prophenoloxidases. BMC biology *13*, 81.

653 Dzik, J.M. (2014). Evolutionary roots of arginase expression and regulation. Frontiers in
654 immunology *5*, 544.

655 Estevez-Lao, T.Y., and Hillyer, J.F. (2014). Involvement of the Anopheles gambiae Nimrod gene
656 family in mosquito immune responses. Insect biochemistry and molecular biology *44*, 12-22.

657 Fossett, N., Hyman, K., Gajewski, K., Orkin, S.H., and Schulz, R.A. (2003). Combinatorial
658 interactions of serpent, lozenge, and U-shaped regulate crystal cell lineage commitment during
659 Drosophila hematopoiesis. Proceedings of the National Academy of Sciences of the United States
660 of America *100*, 11451-11456.

661 Frolet, C., Thoma, M., Blandin, S., Hoffmann, J.A., and Levashina, E.A. (2006). Boosting NF-
662 kappaB-dependent basal immunity of Anopheles gambiae aborts development of Plasmodium
663 berghei. Immunity *25*, 677-685.

664 Gaublomme, J.T., Yosef, N., Lee, Y., Gertner, R.S., Yang, L.V., Wu, C., Pandolfi, P.P., Mak, T.,
665 Satija, R., Shalek, A.K.*, et al.* (2015). Single-Cell Genomics Unveils Critical Regulators of Th17
666 Cell Pathogenicity. Cell *163*, 1400-1412.

667 Gray, E.E., Friend, S., Suzuki, K., Phan, T.G., and Cyster, J.G. (2012). Subcapsular sinus
668 macrophage fragmentation and CD169+ bleb acquisition by closely associated IL-17-committed
669 innate-like lymphocytes. PloS one *7*, e38258.

670 Grun, D., Lyubimova, A., Kester, L., Wiebrands, K., Basak, O., Sasaki, N., Clevers, H., and van
671 Oudenaarden, A. (2015). Single-cell messenger RNA sequencing reveals rare intestinal cell
672 types. Nature *525*, 251-255.

673 Headland, S.E., Jones, H.R., D'Sa, A.S., Perretti, M., and Norling, L.V. (2014). Cutting-edge
674 analysis of extracellular microparticles using ImageStream(X) imaging flow cytometry. Sci Rep *4*,
675 5237.

676 Hernandez, S., Lanz, H., Rodriguez, M.H., Torres, J.A., Martinez-Palomo, A., and Tsutsumi, V.
677 (1999). Morphological and cytochemical characterization of female Anopheles albimanus
678 (Diptera: Culicidae) hemocytes. Journal of medical entomology *36*, 426-434.

679 Hillyer, J.F. (2010). Mosquito immunity. Advances in experimental medicine and biology *708*, 218-
680 238.

681 Hillyer, J.F., and Christensen, B.M. (2002). Characterization of hemocytes from the yellow fever
682 mosquito, Aedes aegypti. Histochemistry and cell biology *117*, 431-440.

683 Hillyer, J.F., Schmidt, S.L., and Christensen, B.M. (2003). Rapid phagocytosis and melanization
684 of bacteria and Plasmodium sporozoites by hemocytes of the mosquito Aedes aegypti. The
685 Journal of parasitology *89*, 62-69.

686 Hillyer, J.F., and Strand, M.R. (2014). Mosquito hemocyte-mediated immune responses. Current
687 Opinion in Insect Science.

688 Hulsmans, M., Clauss, S., Xiao, L., Aguirre, A.D., King, K.R., Hanley, A., Hucker, W.J., Wulfers,
689 E.M., Seemann, G., Courties, G.*, et al.* (2017). Macrophages Facilitate Electrical Conduction in
690 the Heart. Cell *169*, 510-522 e520.

691 Ilicic, T., Kim, J.K., Kolodziejczyk, A.A., Bagger, F.O., McCarthy, D.J., Marioni, J.C., and
692 Teichmann, S.A. (2016). Classification of low quality cells from single-cell RNA-seq data. Genome
693 Biol *17*, 29.

694 King, J.G., and Hillyer, J.F. (2012). Infection-induced interaction between the mosquito circulatory
695 and immune systems. PLoS pathogens *8*, e1003058.

696 King, J.G., and Hillyer, J.F. (2013). Spatial and temporal in vivo analysis of circulating and sessile
697 immune cells in mosquitoes: hemocyte mitosis following infection. BMC biology *11*, 55.

698 Kowal, J., Arras, G., Colombo, M., Jouve, M., Morath, J.P., Primdal-Bengtson, B., Dingli, F., Loew,
699 D., Tkach, M., and Thery, C. (2016). Proteomic comparison defines novel markers to characterize

700 heterogeneous populations of extracellular vesicle subtypes. Proceedings of the National
701 Academy of Sciences of the United States of America *113*, E968-977.

702 Lavine, M.D., and Strand, M.R. (2002). Insect hemocytes and their role in immunity. Insect
703 biochemistry and molecular biology *32*, 1295-1309.

704 Lawson, D., Arensburger, P., Atkinson, P., Besansky, N.J., Bruggner, R.V., Butler, R., Campbell,
705 K.S., Christophides, G.K., Christley, S., Dialynas, E.*, et al.* (2007). VectorBase: a home for
706 invertebrate vectors of human pathogens. Nucleic Acids Res *35*, D503-505.

707 Lombardo, F., Ghani, Y., Kafatos, F.C., and Christophides, G.K. (2013). Comprehensive genetic
708 dissection of the hemocyte immune response in the malaria mosquito Anopheles gambiae. PLoS
709 pathogens *9*, e1003145.

710 Love, M.I., Huber, W., and Anders, S. (2014). Moderated estimation of fold change and dispersion
711 for RNA-seq data with DESeq2. Genome Biol *15*, 550.

712 Michel, K., Budd, A., Pinto, S., Gibson, T.J., and Kafatos, F.C. (2005). Anopheles gambiae
713 SRPN2 facilitates midgut invasion by the malaria parasite Plasmodium berghei. EMBO reports *6*,
714 891-897.

715 Minakhina, S., Tan, W., and Steward, R. (2011). JAK/STAT and the GATA factor Pannier control
716 hemocyte maturation and differentiation in Drosophila. Developmental biology *352*, 308-316.

717 Ottaviani, E., and Franceschi, C. (1997). The invertebrate phagocytic immunocyte: clues to a
718 common evolution of immune and neuroendocrine systems. Immunology today *18*, 169-174.

719 Picelli, S., Bjorklund, A.K., Faridani, O.R., Sagasser, S., Winberg, G., and Sandberg, R. (2013).
720 Smart-seq2 for sensitive full-length transcriptome profiling in single cells. Nat Methods *10*, 1096-
721 1098.

722 Pinto, S.B., Lombardo, F., Koutsos, A.C., Waterhouse, R.M., McKay, K., An, C., Ramakrishnan,
723 C., Kafatos, F.C., and Michel, K. (2009). Discovery of Plasmodium modulators by genome-wide
724 analysis of circulating hemocytes in Anopheles gambiae. Proceedings of the National Academy
725 of Sciences of the United States of America *106*, 21270-21275.

726 Ratajczak, J., Miekus, K., Kucia, M., Zhang, J., Reca, R., Dvorak, P., and Ratajczak, M.Z. (2006).
727 Embryonic stem cell-derived microvesicles reprogram hematopoietic progenitors: evidence for
728 horizontal transfer of mRNA and protein delivery. Leukemia *20*, 847-856.

729 Ribeiro, C., and Brehelin, M. (2006). Insect haemocytes: what type of cell is that? J Insect Physiol
730 *52*, 417-429.

731 Rodrigues, J., Brayner, F.A., Alves, L.C., Dixit, R., and Barillas-Mury, C. (2010). Hemocyte
732 differentiation mediates innate immune memory in Anopheles gambiae mosquitoes. Science *329*,
733 1353-1355.

734 Shalek, A.K., Satija, R., Adiconis, X., Gertner, R.S., Gaublomme, J.T., Raychowdhury, R.,
735 Schwartz, S., Yosef, N., Malboeuf, C., Lu, D.*, et al.* (2013). Single-cell transcriptomics reveals
736 bimodality in expression and splicing in immune cells. Nature *498*, 236-240.

737 Shalek, A.K., Satija, R., Shuga, J., Trombetta, J.J., Gennert, D., Lu, D., Chen, P., Gertner, R.S.,
738 Gaublomme, J.T., Yosef, N.*, et al.* (2014). Single-cell RNA-seq reveals dynamic paracrine control
739 of cellular variation. Nature *510*, 363-369.

740 Smith, R.C., Barillas-Mury, C., and Jacobs-Lorena, M. (2015). Hemocyte differentiation mediates
741 the mosquito late-phase immune response against Plasmodium in Anopheles gambiae.
742 Proceedings of the National Academy of Sciences of the United States of America *112*, E3412-
743 3420.

744 Smith, R.C., King, J.G., Tao, D., Zeleznik, O.A., Brando, C., Thallinger, G.G., and Dinglasan, R.R.
745 (2016). Molecular profiling of phagocytic immune cells in Anopheles gambiae reveals integral
746 roles for hemocytes in mosquito innate immunity. Mol Cell Proteomics.

747 Tassetto, M., Kunitomi, M., and Andino, R. (2017). Circulating Immune Cells Mediate a Systemic
748 RNAi-Based Adaptive Antiviral Response in Drosophila. Cell *169*, 314-325 e313.

749 Tsao, I.Y., Chen, J.W., Li, C.J., Lo, H.L., Christensen, B.M., and Chen, C.C. (2015). The dual
750 roles of Armigeres subalbatus prophenoloxidase V in parasite melanization and egg chorion
751 melanization in the mosquito Ar. subalbatus. Insect biochemistry and molecular biology *64*, 68-
752 77.

753 Tsao, I.Y., Lin, U.S., Christensen, B.M., and Chen, C.C. (2009). Armigeres subalbatus
754 prophenoloxidase III: Cloning, characterization and potential role in morphogenesis. Insect
755 biochemistry and molecular biology *39*, 96-104.

756 Valadi, H., Ekstrom, K., Bossios, A., Sjostrand, M., Lee, J.J., and Lotvall, J.O. (2007). Exosome-
757 mediated transfer of mRNAs and microRNAs is a novel mechanism of genetic exchange between
758 cells. Nat Cell Biol *9*, 654-659.

759 Van De Bor, V., Zimniak, G., Papone, L., Cerezo, D., Malbouyres, M., Juan, T., Ruggiero, F., and
760 Noselli, S. (2015). Companion Blood Cells Control Ovarian Stem Cell Niche Microenvironment
761 and Homeostasis. Cell reports *13*, 546-560.

762 van der Pol, E., Boing, A.N., Harrison, P., Sturk, A., and Nieuwland, R. (2012). Classification,
763 functions, and clinical relevance of extracellular vesicles. Pharmacol Rev *64*, 676-705.

764 Vlisidou, I., and Wood, W. (2015). Drosophila blood cells and their role in immune responses.
765 FEBS J *282*, 1368-1382.

766 Volohonsky, G., Hopp, A.K., Saenger, M., Soichot, J., Scholze, H., Boch, J., Blandin, S.A., and
767 Marois, E. (2017). Transgenic Expression of the Anti-parasitic Factor TEP1 in the Malaria
768 Mosquito Anopheles gambiae. PLoS pathogens *13*, e1006113.

769 Volohonsky, G., Terenzi, O., Soichot, J., Naujoks, D.A., Nolan, T., Windbichler, N., Kapps, D.,
770 Smidler, A.L., Vittu, A., Costa, G.*, et al.* (2015). Tools for Anopheles gambiae Transgenesis. G3
771 (Bethesda) *5*, 1151-1163.

772 WHO (2014). A global brief on vector-borne diseases, W.H. Organization, ed. (Geneva,
773 Switzerland: WHO Press).

774 Wood, W., and Jacinto, A. (2007). Drosophila melanogaster embryonic haemocytes: masters of
775 multitasking. Nat Rev Mol Cell Biol *8*, 542-551.

776 Wu, A.R., Neff, N.F., Kalisky, T., Dalerba, P., Treutlein, B., Rothenberg, M.E., Mburu, F.M.,
777 Mantalas, G.L., Sim, S., Clarke, M.F.*, et al.* (2014). Quantitative assessment of single-cell RNA-
778 sequencing methods. Nat Methods *11*, 41-46.

779 Xue, Z., Huang, K., Cai, C., Cai, L., Jiang, C.Y., Feng, Y., Liu, Z., Zeng, Q., Cheng, L., Sun, Y.E.,
780 *et al.* (2013). Genetic programs in human and mouse early embryos revealed by single-cell RNA
781 sequencing. Nature *500*, 593-597.

782 Yassine, H., Kamareddine, L., and Osta, M.A. (2012). The mosquito melanization response is
783 implicated in defense against the entomopathogenic fungus Beauveria bassiana. PLoS
784 pathogens *8*, e1003029.

785 Zdobnov, E.M., von Mering, C., Letunic, I., Torrents, D., Suyama, M., Copley, R.R., Christophides,
786 G.K., Thomasova, D., Holt, R.A., Subramanian, G.M., *et al.* (2002). Comparative genome and
787 proteome analysis of Anopheles gambiae and Drosophila melanogaster. Science *298*, 149-159.

788

789

790 **MATERIALS and METHODS**

791 **Mosquito rearing, fluorescence microscopy and hemolymph perfusion**

792 *Anopheles gambiae sensu lato PPO6::RFP* transgenic (Volohonsky et al., 2015) and wild type
793 strains were reared at 28°C, under 80% humidity and at a 12/12 h day/night cycle. Larvae were
794 fed with cat food and adult mosquitoes were fed *ad libitum* with 10% sugar solution. For tissue
795 microscopy, adult female mosquitoes were dissected in 1 X PBS, fixed in 4% paraformaldehyde
796 (PFA), washed three times and mounted using Vectashield mounting medium containing DAPI.
797 For hemolymph perfusion, 3-5-day-old female mosquitoes were anesthetized on ice for 10 min,
798 microinjected with 700 nl of a buffer containing 60% Schneider's Medium, 10% fetal bovine serum
799 (FBS), and 30% citrate buffer (anticoagulant; 98 mM NaOH, 186 mM NaCl, 1.7 mM EDTA, 41
800 mM citric acid, pH 4.5) and allowed to rest, on ice, for 10 min. A small cut was made between the
801 last two abdominal segments with the help of dissection scissors and the flow through was
802 collected after further injection of 10 µl of buffer. For microscopy analyses, mosquitoes were
803 perfused directly onto glass slides or coverslips, and cells were allowed to attach for at least 15
804 min prior to fixation in 4% PFA. Cells were next stained with a 1:100 dilution of Alexa 488
805 Phalloidin (ThermoFisher) for 30 min at room temperature. For the DiD analyses, cells were
806 stained with DiD (5 µM) for 20 min prior to PFA fixation. Following washes, cells were mounted
807 as described above, and analyzed on a Zeiss Axiovert microscope.

808

809 **FACS and single-cell RNA-sequencing by SMART-Seq2**

810 For FACS and imaging flow cytometry analyses, 10-12 mosquitoes were perfused. Hemolymph
811 perfusate was collected with the help of a pipette, transferred into a siliconized microtube and
812 diluted to a final volume of 500 µl buffer containing 2 µg/ml of Hoechst 3342 (Molecular Probes).
813 Cells were immediately analyzed in a BD ARIA II Cell Sorter equipped with violet and green-
814 yellow lasers at 405 and 561 nm, respectively. Cells were first gated based on their RFP
815 fluorescence, followed by positive Hoechst signal, with Area versus Width measurements being
816 used for doublet discrimination. The FACS machine was standardized with fluorochrome-
817 containing beads and sorting purity was validated by visualization of cells sorted onto a glass
818 coverslip. Cells were sorted into a 96-well PCR plate containing 5 µl of 0.2% Triton X-100
819 supplemented with 2 U/µl of RNAse inhibitor (Clontech), with two wells containing 30 cells each
820 (pool samples) and one column (8 wells) containing only the lysis buffer used as a negative
821 control. We added ERCC spike-ins (Ambion) at a 1:2 billion dilution into the plate prior to cDNA
822 synthesis and all samples were next processed according to the SMART-Seq2 protocol using up
823 to 22 PCR cycles for cDNA synthesis (Picelli et al., 2013). PCR products were purified with
824 AMPure XP beads (Beckman Coulter). Quality control was performed for each sample individually
825 both as cDNA input and sequencing library using a high sensitivity DNA kit (Agilent). A total of
826 125 pg of cDNA was used for library construction. cDNA libraries were pooled at a 10nM final
827 concentration and 100 bp paired end sequencing was performed in one lane using a HiSeq2000
828 Sequencer (Illumina).

829

830 **RNA-seq data analysis**

831 Reads generated by sequencing were demultiplexed using bcl2fastq (version 1.8.4) and mapped
832 to *A. gambiae* genome (P4), ERCC92 (Ambion) and *dTomato* sequence (Volohonsky et al., 2015)
833 with the STAR aligner (version 2.4.2a) (Dobin et al., 2013). The genome index was generated
834 with *A. gambiae* geneset file in gtf format (P4.4) and gene count tables were produced during the
835 mapping (--quantMode Genecounts). They were next normalized with size factors calculated from
836 the ERCCs using DESeq2 (Love et al., 2014). For the purpose of comparisons, a gene was
837 considered expressed if at least one normalized read was identified in at least one sample. Genes

838 were annotated using Vectorbase (Lawson et al., 2007) and manual curation. For comparisons
839 with previous studies (Baton et al., 2009; Pinto et al., 2009; Smith et al., 2016), gene IDs were
840 converted using Vectorbase and BioMart. Intersection analyses were performed in R using the
841 VennDiagram and upsetR packages. Technical noise estimation and identification of the highly
842 variable genes were performed as reported before (Brennecke et al., 2013), using the 60-
843 percentile as the mean cut-off to include more ERCC genes in the technical fit. Principal
844 component analyses were done with the *prcomp* function and differential expression analyses
845 were based on the DESeq2 package, using the ERCC size factors and $PPO6^{low}$ versus $PPO6^{high}$
846 as comparison. For GO analyzes, we used topGO (Alexa et al., 2006) and GO terms were
847 obtained from the org.Ag.eg.db annotation package. Analyses were performed in R and scripts
848 are available upon request. The sequencing results were deposited in the European Nucleotide
849 Archive under the following accession number: PRJEB23372 and the processed expression data
850 can be accessed at http://data.teichlab.org for single gene visualization.

851

852 **Imaging flow cytometry**

853 Ten to twelve sugar-fed *PPO6::RFP* female mosquitoes were perfused to a final volume of 20-40
854 µl and the diluted hemolymph samples were immediately analyzed in an Amnis ImageStreamX
855 MKII (Merck). For *PPO6::RFP* analyses, wild type mosquitoes were used to set background
856 fluorescence and cells were measured with a 40x objective. Comparisons between cell
857 subpopulations were performed using the "Object" mask and based on a built-in function that uses
858 Fisher's discriminant ratio (Rd) to determine the best statistical separation (largest Rd) between
859 identified populations. For the DiD analyses, cells were collected into FBS-free buffer containing
860 1 µM of DiD and analyzed at 60x to increase resolution. Single staining controls representing
861 RFP, DiD and medium alone were used for calibration and manual compensation. Experiments
862 were repeated at least twice. Cell gating was confirmed considering the obtained images and
863 manually curated to exclude debris and doublets that could not be excluded by the gating alone.
864 Vesicle detection was performed as reported before (Headland et al., 2014). Briefly, DiD positive
865 events were interrogated based on their level of DiD fluorescence and size scatter intensity. DiD-
866 labelled vesicles showed a low scatter along with low to mid DiD fluorescence, whereas cells
867 displayed mid to high fluorescence and scatter measurements. Speed beads, used for the
868 instrument calibration and focusing, were easily gated out as a discrete population displaying very
869 high levels of side-scatter intensity. The RFP intensity was measured based on the median pixel

870 by means of histogram, and cellular debris and doublets were excluded according to their
871 brightfield area and aspect ratio. The identified populations were compared using the "Feature
872 Finder" function of the IDEAS software (MilliporeSigma). Statistical analyses were based on
873 Mann-Whitney-Wilcoxon and graphs were done in R.

874

875 **RNA *in situ* hybridization using RNAscope**

876 RNA *in situ* studies were performed according to the RNAscope Multiplex Fluorescence analyses
877 manual (Advanced Cell Diagnostics). Briefly, cells were perfused onto glass slides, allowed to
878 attach and fixed in PFA as described above. If needed, slides were dehydrated and kept in 100%
879 ethanol at -20˚C until processing. Samples from *A. stephensi* were handled following the same
880 procedure. Tissue samples were processed immediately after dissection in RNAse-free PBS. All
881 RNAscope probes were designed by Advanced Cell Diagnostics and are commercially available.
882 Each probe was individually tested against a negative control prior and during each analysis.
883 Images were acquired using a Leica SP8 confocal microscope equipped with 405, 488, 561 and
884 647 nm lasers and prepared for submission using the basic features of the LAS X software.

885

886 **Bead uptake assay**

887 For magnetic isolation of hemocytes, we followed the protocol by Smith et al 2016 with small
888 modifications. Briefly, 20 female mosquitoes were cold anesthetized and injected with 300 µl of a
889 2 mg/ml suspension of MagnaBind Carboxyl Derivatized Beads (Thermo Scientific). Mosquitoes
890 were next kept at 28°C or 4°C for 2 h and perfused as described above. Hemolymph perfused
891 was collected with the help of a pipette tip and transferred into a 0.5 µl Eppendorf tube containing
892 100 ul of injection buffer. Samples were diluted to 200 µl and incubated in a magnetic stand for
893 20 min at 4°C. Supernatant was removed by pipetting, magnetic pellet was resuspended in 1 X
894 RNAse-free PBS and transferred to a microscopy slide. Cells were allowed to attach for 15 min
895 and processed for RNA-FISH as described above.

896

897 **Transwell assay**

898 For this assay, we used *PPO6::RFP* transgenic mosquitoes and the *A. gambiae* Ngousso
899 (TEP1*S1) wild-type mosquito strain. Perfusion was performed in the absence of FBS and
900 hemolymph was collected with the help of a pipette onto the top of a glass coverslip placed inside
901 a 24-well plate. A total of 100 µl of buffer was further gently pipetted onto the cell drop to prevent
902 dehydration. Cell inserts (Merck) were then placed over individual wells and hemolymph perfusate
903 from *PPO6::RFP* female mosquitoes was gently pipetted onto the 1 µm membrane mesh. Diluted
904 hemolymph from at least 2 wild type and 4 transgenic mosquitoes were used per treatment, and
905 the negative control consisted of overlaying coverslips with buffer only. Plates were kept at room
906 temperature for at least 1 h; following by fixation of coverslips with 4% PFA and PBS washes prior
907 to immediate processing based on the RNAscope manual. Images were obtained by confocal
908 microscopy as described above. Experiments were repeated at least twice.

909

910 **Scanning electron microscopy:**

911 For scanning electron microscopy (SEM), cells were perfused from at least 2 female mosquitoes
912 directly onto glass coverslips and fixed with 4% PFA. To facilitate exosome imaging, poly-L-lysine
913 treated coverslips were used. For correlative SEM, cells were placed onto microscopic dishes
914 with finder grids (ibidi) and imaged directly after 4% PFA fixation using a Zeiss Axiovert
915 microscope, prior to SEM processing. The samples were post-fixed in 2.5% glutaraldehyde, 0.5%
916 osmium-tetroxide, tannic acid and osmium-tetroxide again. The coverslips or optical membranes
917 were then dehydrated in a graded ethanol series, dried in carbon dioxide at critical point and
918 vacuum coated with 3 nm Carbon-Platinum. Imaging was performed using a LEO 1550 (Zeiss,
919 Oberkochen DE) scanning-electron microscope. Experiments were repeated at least twice.

920

921 **Transmission electron microscopy:**

922 EVs were isolated according to a protocol described before (Kowal et al., 2016). In summary,
923 hemolymph perfusate from at least 20 mosquitoes was subjected to differential centrifugation at
924 4˚C and the 10,000 x g pellet was processed for negative staining electron microscopy. Aliquots
925 of the samples were applied to freshly glow discharged carbon- and pioloform-film-coated copper
926 grids and allowed to adsorb for 10 min. After washes with distilled water, the grids were contrasted
927 with 2% uranyl acetate, touched on filter paper and air-dried. The grids were examined in a LEO

906 (Zeiss AG, Oberkochen) electron microscope operated at 100 kV and images were recorded with a Morada (SIS-Olympus, Münster) digital camera.